2.4 SCALING ANALYSIS OF THE TURBULENT KINETIC ENERGY AT THE ENTRAINMENT ZONE IN SHEARED CONVECTIVE BOUNDARY LAYERS

David Pino *
Applied Physics Department, Technical University of Catalonia, and
Institute for Space Studies of Catalonia (IEEC/CSIC), Barcelona, Spain
Jordi Vilà–Guerau de Arellano
Meteorology and Air Quality Section, Wageningen University, Wageningen, The Netherlands

1. INTRODUCTION

The development and maintenance of a well–mixed atmospheric boundary layer have a direct influence on many atmospheric phenomena, such as cloud formation or pollutant distribution. The growth of the convective boundary layer (CBL) is driven by both surface fluxes of heat and moisture and by the entrainment of warm and dry air from the free atmosphere into the boundary layer. Wind shear at the surface and at the inversion layer enhances these processes. Buoyancy and shear can substantially affect the depth of the mixed layer, the CBL's main characteristics and the turbulence statistics. The structure of the CBL has been theoretically found to differ in purely neutral and convective cases (Sykes and Henn 1989; Moeng and Sullivan 1994; Khanna and Brasseur 1998). Moreover, observations and numerical simulations have shown that in a CBL where both forces are present, the convection pattern is in the form of horizontal rolls (LeMone 1973; Christian and Wakimoto 1989, Pino et al. 2003).

From 1970 onwards many researchers (Tennekes 1973; Stull 1976a; Zeman and Tennekes 1977; Tennekes and Driedonks 1981; Driedonks and Tennekes 1984; Fedorovich 1995; Sorbjan 1996; Pino et al. 2003, 2006; Sorbjan 2004; Kim et al. 2006; Conzemius and Fedorovich 2006b) have concentrated on studying the value and possible evolution of the ratio of virtual potential temperature fluxes at the inversion level and at the surface, $\beta = -\overline{w\theta_v}|_i/\overline{w\theta_v}|_s$. The main goal of these studies was to understand the driving processes of the entrainment heat flux and subsequently to develop a suitable parameterization for the entrainment flux. By analyzing the turbulence kinetic energy (TKE) budget, it is possible to obtain a parametric expression which depends only on scaling parameters. These expressions have been evaluated with observations (Artaz and André 1980; Dubosclard 1980; Driedonks 1982; Culf 1992; Betts and Ball 1994; Angevine et al. 1998; Hägeli et al. 2000). By comparing the parameterized boundary layer depth or entrainment flux ratio against observations, the authors of some of these studies pointed to the importance of taking shear and dissipation contributions into account in the parameterizations.

*Corresponding author address: David Pino, Applied Physics Department, Technical University of Catalonia, Av del Canal Olímpic s/n, 08860 Castelldefels, Spain; e-mail: david@fa.upc.edu

Compared with the previous studies, the main advantage of using large–eddy simulation (LES) is to be able to calculate each of the TKE budget contributions. These previous studies presented and evaluated the final expression of the virtual potential temperature flux ratio and some of them only used mathematical arguments to parameterize each of the terms without taking into account the physical processes involved in the evolution of each particular term of the TKE budget (see Conzemius and Fedorovich (2006b) for a review of the parameterizations). In this research study, following the approach of Zeman and Tennekes (1977) and Tennekes and Driedonks (1981), we focus on the physical aspects of the scaling of each specific TKE budget term.

By varying the wind characteristics of each large–eddy simulation experiment, we were able to evaluate the influence of the shear on the other terms of the TKE budget at the entrainment zone. Subsequently, we applied convective and local (stable) scaling to each term of the TKE budget at the entrainment zone.

This extended abstract summarizes the results presented at Pino and Vilà–Guerau de Arellano (2008).

2. NUMERICAL SETUP

To simulate the evolution of the CBL and to study the importance of the entrainment fluxes in this evolution, we performed five different runs of the Dutch LES model (DALES) described in Cuijpers and Duynkerke (1993) and modified by Cuijpers and Holtslag (1998). In the five simulations, all the initial and boundary conditions were identical except for the values of the geostrophic wind. The first case was defined as a boundary layer driven only by the surface heat flux, without geostrophic wind, namely NS (free convection, no shear). In the rest of the numerical experiments geostrophic wind was progressively increased, namely GC simulations (forced convection). We studied and scaled the LES results of the different contribution of the TKE terms for CBL flows characterized by different geostrophic wind conditions. the value of the constant geostrophic wind increases from 5 m s^{-1} (GC5) to 20 m s^{-1} (GC20) with a 5 m s^{-1} interval in a domain with a surface roughness length $z_0 = 0.15$ m.

Constant values of potential temperature and humidity fluxes $\overline{w\theta}|_s = 0.1$ K m s^{-1} and $\overline{wq}|_s = 0.146$ g kg^{-1} m s^{-1} were prescribed in all the numerical experiments.

A 12.6$\times$12.6$\times$3 km^3 domain with grid spacing $\Delta x = \Delta y = 50$ m and $\Delta z = 12$ m was used. The total simulation time was 8 hours, and the slab horizontal averaged

model output was recorded every five minutes. The final statistics used in this work were obtained by performing a temporal averaging every 30 minutes, i. e. six instants were used.

The initial profiles for potential temperature (Θ) and specific humidity ($\overline{q}$) were based in a previous observational case studied by Pino et al. (2003). The initial mean potential temperature (specific humidity) value for all the simulations is $\Theta_0 = 306$ K ($\overline{q}|_0 = 15.6$ g kg^{-1}, these values correspond to $\Theta_v|_0 = 308.9$ K) below 625 m; it increases by 6 K (decreases by 9.8 g kg^{-1}) up to 825 m, and increases at a constant rate of $\gamma = 2.58$ K km^{-1} (specific humidity has a constant value of 5.8 g kg^{-1}) above this point.

As an indication of the atmospheric boundary layers reproduced in the numerical experiments, the scaling and non–dimensional values are given at Table 1. The values were calculated after averaging between 3.5 and 4 hours in the simulation. The boundary layer height, z_i, is defined as the height of the minimum virtual potential temperature flux; $\delta = h_2 - z_i$, where h_2 is the height where the virtual potential temperature flux goes to zero above z_i; u_*, w_* are the friction and convective scaling velocities. The other variables are defined as follows: $\Theta_* = \overline{w\theta_v}|_s/w_*$, $q_* = \overline{wq}|_s/w_*$, γ_i is the maximum gradient of the virtual potential temperature in the interfacial layer, L is the Monin–Obukhov length and Ri_f is the flux Richardson number. As shown by the decreasing value of Ri_f at Table 1, mechanical turbulence at the entrainment zone becomes an important contribution in the boundary layer development, varying accordingly the values of the scaling variables and non–dimensional numbers.

Run	NS	GC5	GC10	GC15	GC20
z_i (m)	904	896	912	966	1046
δ (m)	180	194	242	292	344
u_* (m s^{-1})	-	0.323	0.508	0.667	0.810
w_* (m s^{-1})	1.541	1.537	1.546	1.576	1.618
Θ_* (K)	0.0835	0.0837	0.0832	0.0817	0.0796
q_* (10^{-5})	9.47	9.49	9.44	9.26	9.02
γ_i (K km^{-1})	15.09	13.27	10.49	9.34	8.65
Ri_f (at z_i)	-	3.83	0.77	0.38	0.32
z_i/L	-	-43.9	-11.5	-5.4	-3.2

Table 1: Averaged scaling values and non–dimensional numbers of the boundary layer and the entrainment zone of the five numerical experiments. The averaged period was between 3.5 and 4 hours of the simulations.

3. RESULTS

3.1 *Mean variables*

In this work no figure showing the vertical profile of any mean variable except TKE is shown. A complete description of the results are written in Pino and Vilà–Guerau de Arellano (2008). The main differences between the five numerical experiments can be summarizes as follows:

- Except for weak wind experiment (GC5), wind shear in the lower and upper boundaries tends to increase the entrainment ratio with respect to the pure buoyancy case (Mahrt and Lenschow 1976; Tennekes and Driedonks 1981; Pino et al. 2003; Sorbjan 2006; Conzemius and Fedorovich 2006a). In GC simulations, β increases during the first hours due to the increase of wind shear at the inversion. Afterwards, once entrainment wind shear is approximately constant or gently decreases, β slowly decreases its value. The classical value for shearless CBL $\beta = 0.2$ is still a good approximation for NS and even GC5 cases. For the studied cases, where the boundary layer is already developed and the entrainment zone is far above the surface ($z_i|_0 = 750$ m), the initial increase of β observed in all the studied cases can not have been caused by the proximity to the surface which enhances transport of surface shear TKE to the entrainment zone (Conzemius and Fedorovich 2006a). In these numerical experiments, this is only caused by the appearance of shear generated turbulence at the inversion.

- The geostrophic wind increase leads to a larger gradient of both wind components in the boundary layer, and an increase in the entrainment of momentum. Furthermore, the v–component is not as well mixed as u–component. Consequently, a less mixed velocity field in the boundary layer is found.

- Due to the enhancement of entrainment fluxes, a warmer and drier boundary layer is found with increasing geostrophic wind.

- Geostrophic wind also enhances boundary layer growth and enlarges the interfacial layer. Sheared CBLs, except GC5, grow faster than the pure buoyancy CBL (NS case). GC5 gives similar values of z_i, or even lower, at the beginning of the simulation than the NS case for this value of $\overline{w\theta}|_s$. This fact serves as evidence in supporting the theory of shear sheltering of turbulence (Hunt and Durbin 1999; Fedorovich et al. 2001). This effect is associated with the blockage of turbulence propagation through an interface between turbulent and non–turbulent flows caused by shear. Regarding the inversion layer thickness, shear enhances its growth. In all cases δ increases with time. Only for GC15 and GC20 some fluctuations appeared in δ growth at the end of the simulation.

- Since the surface potential temperature flux is kept constant in the simulations, the amount of heat introduced in the mixed layer can only vary due to the entrainment of warm air from the free troposphere. Therefore, the positive part of the total integral of the virtual potential temperature flux, P_f, only depends on the value of h_0 (height where the virtual potential temperature flux is zero below z_i). The five studied cases produce similar values of h_0 and P_f. However,

the area of the negative virtual potential temperature flux, which is proportional to the amount of heat entrained from the free atmosphere, can be smaller for GC5 case, due to shear sheltering of turbulence, and as much as five times larger for the GC20 case than in the pure buoyancy case.

3.2 *Turbulence kinetic energy budget*

The following step is to determine how shear at the entrainment zone modifies the turbulence kinetic energy. Under horizontally homogeneous conditions and in absence of mean subsidence, the turbulence kinetic energy budget reads:

$$\frac{\partial \overline{e}}{\partial t} = -\left[\overline{uw}\frac{\partial U}{\partial z} + \overline{vw}\frac{\partial V}{\partial z}\right] + \frac{g}{\Theta_{vr}}\overline{w\theta_v} - \frac{\partial \overline{we}}{\partial z} - \frac{1}{\rho_0}\frac{\partial \overline{wp}}{\partial z} - \epsilon, \quad (1)$$

where (u, v, w) are the fluctuating velocity components; U, V are the horizontal components of the mean wind, p is the pressure, ρ_0 is a reference density, Θ_{vr} is a reference virtual potential temperature, $\overline{e} = 0.5(\overline{u^2} + \overline{v^2} + \overline{w^2})$ is the mean turbulence kinetic energy (Stull 1988), and ϵ is the viscous dissipation of TKE. The term on the left–hand side represents the time tendency of TKE (TE), and the terms on the right–hand side are the shear production (S), the buoyancy production (B), the turbulent transport (T), the pressure correlation (P) and the viscous dissipation term (ϵ). The first term on the right–hand side is a source, P and T only redistribute the TKE vertically and the last one is a sink. Usually, terms T and P are considered together as the convergence of the turbulence kinetic energy flux (Driedonks 1982).

The total TKE budget for the five analyzed cases after 4 hours of simulation is shown in figure 1. In the TKE budget of the NS simulation (figure 1a), the primary source term in the boundary layer is the buoyancy production. In absence of shear, under quasi–steady–state conditions there is a balance between the sum of the dissipation and buoyancy terms and the pressure and transport contributions at the inversion ($B + \epsilon = T + P$). When mean wind is included in the experiments (figures 1b–e), the TKE budget is clearly modified. When the geostrophic wind value increases from 5 to 20 m s^{-1}:

- Unless very large values of wind are considered ($U_0 \geq 15$ m s^{-1}), wind shear is mainly localized at the surface and at the inversion zone. Note that in all of the cases, although wind shear only occurs at the surface, a shear contribution develops at the inversion zone but remains very small in the middle of the CBL. This is because surface fluxes generate large eddies that can effectively mix the mean winds in the middle of the CBL reducing $\partial U/\partial z$ and hence reducing the shear production (Moeng and Sullivan 1994).

- The minimum of the buoyancy term decreases with respect to simulation NS at the inversion level, but hardly changes in the middle of the CBL. The mean value of β during the eight hours of simulation varies from 0.17 for NS to 0.32 for GC20.

- In order to balance the shear production at the surface and at the entrainment zone, the dissipation increases its absolute value. When low values of the geostrophic wind are considered, dissipation is nearly uniform with height except when it is very close to the surface and at the entrainment zone.

- The sum of the pressure and transport terms reduces its contribution in the whole boundary layer except at the surface. Therefore surface shear is not transported upwards probably because it is locally dissipated at the surface (Lenschow 1970, 1974; Deardorff and Willis 1982; Moeng and Sullivan 1994; Conzemius and Fedorovich 2006a). As a consequence, most of the shear that exists at the entrainment zone is locally created. As will be shown in section 3.4, at the entrainment zone, the term $T + P$ can even become a destruction term (see the decrease of the term from figure 1a to 1e). This means that upward buoyancy transport is suppressed by the downward transport of shear generated TKE. The evolution of the vertical profiles of the two terms T and P is now analyzed separately. The pressure term is small around z_i for all the simulated cases. For NS and GC5 cases, during the whole simulated period, except near the surface, it is negative below z_i changing sign around the mixed–layer depth. When wind shear increases ($U_0 \geq 10$ m s^{-1}) it reduces its value and after two hours of simulation it becomes a destruction term in the boundary layer except near the surface. On the other hand, the transport term is always positive in the upper part of the boundary layer. However, its value decreases in the entrainment zone with increasing shear by means of the physic mechanism explained above in this point.

- As can be observed, the tendency term TE remains small for all the cases.

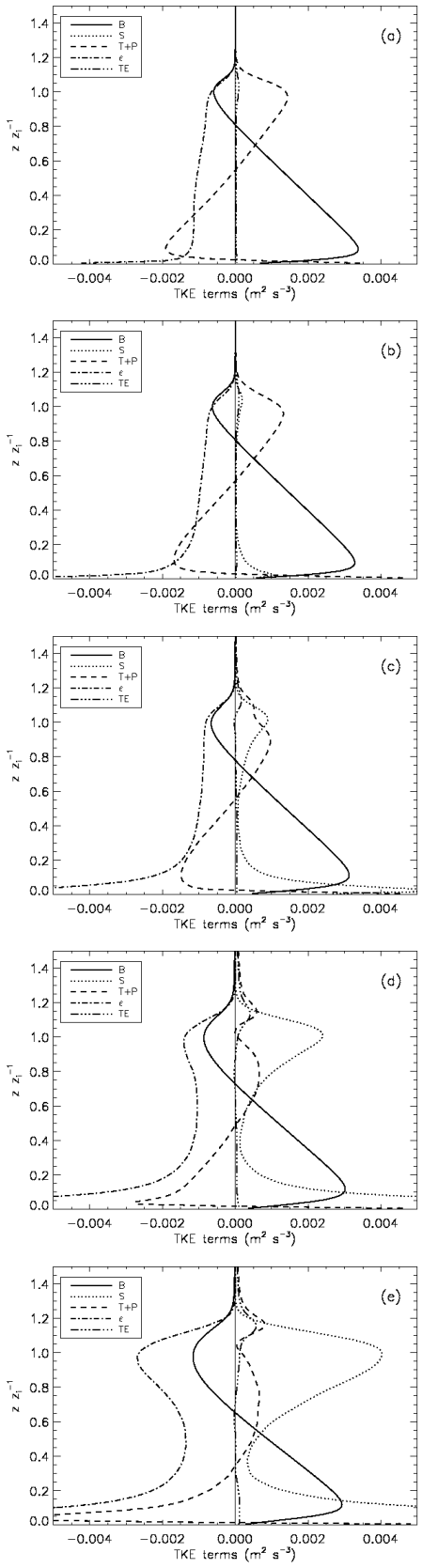

FIGURE 1: Vertical distributions of the various terms (buoyancy–B, dissipation–ϵ, transport and pressure–$T + P$, storage–TE, and shear–S) of the TKE budget for (a) NS, (b) GC5, (c) GC10, (d) GC15, and (e) GC20 30 minutes averaged after 4 hours of simulation. The height is normalized by the mixed–layer depth, z_i.

3.3 *Flux Richardson number*

Prior to the scaling of the TKE terms at the entrainment zone, it is interesting to study the characteristics of the turbulence in the simulated cases in order to identify different turbulent regimes. Following previous studies (Mahrt and Lenschow 1976; Kim et al. 2003; Sorbjan 2004; Conzemius and Fedorovich 2006a), we calculate the flux Richardson number defined as:

$$Ri_f = \frac{(g/\Theta_v)\,\overline{w\theta_v}}{\overline{uw}\,(\partial U/\partial z) + \overline{vw}\,(\partial V/\partial z)}. \qquad (2)$$

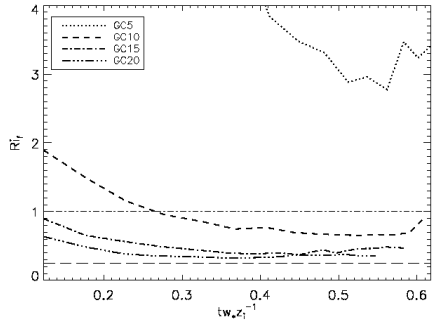

FIGURE 2: Averaged flux Richardson number (Ri_f) at $z = z_i$ as a function of $tw_* z_i^{-1}$ for all the sheared simulated cases. The horizontal lines are drawn at $Ri_f = 0.25$ (dashed) and $Ri_f = 1$ (dash–dotted).

In order to illustrate the atmosphere stability during the whole simulated period, figure 2 shows the time evolution Ri_f at z_i. Whereas the entrainment zone at GC5 is characterized by a strong stratification, for the rest of the sheared cases shear generated turbulence increases atmosphere instability after 2 hours of simulation, being $Ri_f < 1$ but $Ri_f > 0.25$. Therefore, due to the differences in the atmosphere stability at the entrainment zone of the simulated cases, the TKE terms of NS and GC5 simulations might obey different scaling laws that the corresponding terms in GC10, GC15 and GC20 cases. In this sense, the GC5 simulation does not introduce any particular new feature in the boundary layer evolution with respect to the NS case, as discussed in section 3.1.

3.4 *Scaling of the TKE terms*

We finally analyze the time evolution of each TKE term at z_i. Moreover, we apply physical arguments to scale each term. For any term of the TKE budget the contribution of convective scales, based on the bulk mixed–layer properties, and local scales at the entrainment zone are applied. A similar approach was followed by Sorbjan (2005, 2006) to parameterize LES vertical profiles for free and forced convection cases. To our knowledge, this is the first time that any of the TKE terms are scaled separately for convective boundary layers with different shear contributions and verified through the use of LES results. Once any TKE term is scaled, a parameterization for the

entrainment of the virtual potential temperature flux is derived following (1). By scaling each term in the TKE equation, one is able to calculate the buoyancy term as a function of the other contributions: $-B = -TE+S+T+P+\epsilon$. As mentioned before, the TE term, which has been historically parameterized by using a velocity scale, which includes friction and convective velocities, and z_i as length scale (Zilitinkevich 1975, 1991; Pino et al. 2003), is not considered because, at the inversion, it is negligible in all the studied cases.

3.4.1 Shear contribution

Stull (1976b, 1988) discussed the role of mechanical turbulence generated by wind shear at the surface and at the inversion level in the entrainment process. He concluded that for winds roughly above 5 m s^{-1}, buoyancy is not the only factor that contributes to the development of the CBL. When large shear exists at the inversion, the produced mechanical turbulence is not totally locally dissipated, and the condition $\epsilon = S$ is not satisfied (see figure 1e). It is therefore advisable to represent the contribution made to the TKE budget by the turbulence produced by local wind shear at the top of the mixed layer. Although previous authors have proposed z_i as the length scale for this term (Tennekes and Driedonks 1981; Driedonks 1982; Pino et al. 2003; Kim et al. 2006), if its contribution is locally produced, the natural length scale is the inversion layer thickness, δ. Regarding the velocity scale, two possible options naturally appear. Most of the authors used ΔV_e, the modulus of the velocity jump on each horizontal direction, ΔU and ΔV, at the inversion base, and the entrainment velocity in absence of subsidence, $w_e = \partial z_i/\partial t$. However, in this study, we introduce another possible velocity scale related to the local value of the momentum fluxes at the inversion. Consequently we define:

$$u_*|_i = \left(\overline{uw}|_i^2 + \overline{vw}|_i^2\right)^{0.25}, \qquad (3)$$

where the subscript $|_i$ means its value at z_i. Several types of combinations with these velocity scales have been tested. Inspired from the expression of shear term at the TKE budget equation, we propose:

$$S = C_M u_*|_i^2 \left(\frac{\Delta V_e}{\delta}\right), \qquad (4)$$

with $C_M = 1.15$.

Figure 3 shows the time evolution of shear contribution of the TKE at z_i for all the sheared CBLs obtained by means of LES (asterisks) and by using Eq. (4) (solid line). As shown, shear contribution at the entrainment zone increases, reaches a maximum approximately in the middle of the simulation period and then decreases. This is caused by the evolution of δ (not shown) and ΔV_e or $u_*|_i$. These two velocity–related scales increase at the beginning of the simulation and then remain constant (not shown but explained in section 3.1). As it can be noticed, this term clearly scales with δ, ΔV_e and $u_*|_i$. Therefore Eq. (4) captures satisfactorily the TKE production by shear. Moreover, shear contribution to the TKE in the entrainment zone is not affected by processes in the boundary layer.

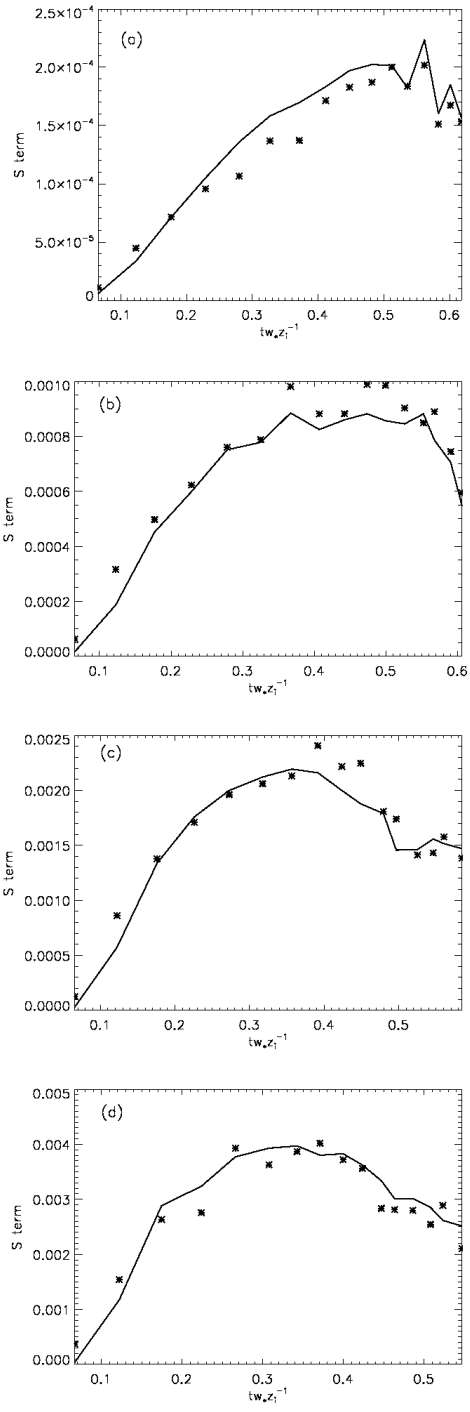

FIGURE 3: Shear (S) contribution to the TKE budget at z_i obtained by LES (asterisks) and by means of Eq. (4) (solid line) as a function of $tw_*z_i^{-1}$ for (a) GC5, (b) GC10, (c) GC15, and (d) GC20 cases.

3.4.2 TRANSPORT AND PRESSURE CONTRIBUTIONS

Classically, this term was only scaled by using convective mixed–layer parameters, without considering local processes at the entrainment zone (Tennekes 1973, 1975; Tennekes and Driedonks 1981). However, as we found in figure 1, shear contribution at the inversion largely modifies $T + P$. From this figure, it is clear that, at the inversion, $T + P$ decreases when the S term increases. Therefore, $T + P$ is also influenced by local processes which vary its value similarly to the shear term. These local processes can scale with δ, ΔV_e, and $u_*|_i$. The proposed parameterization has therefore two different contributions:

$$T + P = TP_{NL} + TP_L. \tag{5}$$

The first one is the positive non–local contribution of spinning up the entrained air to the turbulent levels in the boundary layer. Therefore, using previous studies (Tennekes 1973, 1975), we scaled it as:

$$TP_{NL} = C_F \frac{w_*^3}{z_i}, \tag{6}$$

with $C_F = 0.35$. This constant is larger than the classical closure value for pure convective boundary layer, 0.2. In this later case, the negative dissipation contribution is implicitly included. That is, some of the transport contribution is locally dissipated at the entrainment zone. As a consequence, in the classical closure, the dissipation contribution which was not explicitly considered in the entrainment zone, is supposed to scale at least with w_* and z_i.

Moreover, as shown in figure 1, $T + P$ term in the entrainment zone decreases when shear is introduced in the simulations. A similar behavior is found if the two terms are considered separately (not shown). Both pressure and transport terms at z_i largely decreases with increasing shear, being the pressure term negative for cases GC10, GC15 and GC20 after two hours of simulation approximately. For this reason, we postulate the existence of a negative local contribution due to the horizontal movements caused by the downward transport of shear generated TKE that inhibits the upward vertical transport of TKE and reduces $T + P$ term at z_i. This negative contribution, which increases with wind shear in the entrainment zone, is scaled by using local values:

$$TP_L = -C_P \frac{u_*|_i^3}{\delta}, \tag{7}$$

with $C_P = 5$. It is important to notice that this negative contribution is only important when significant wind shear exists across the inversion.

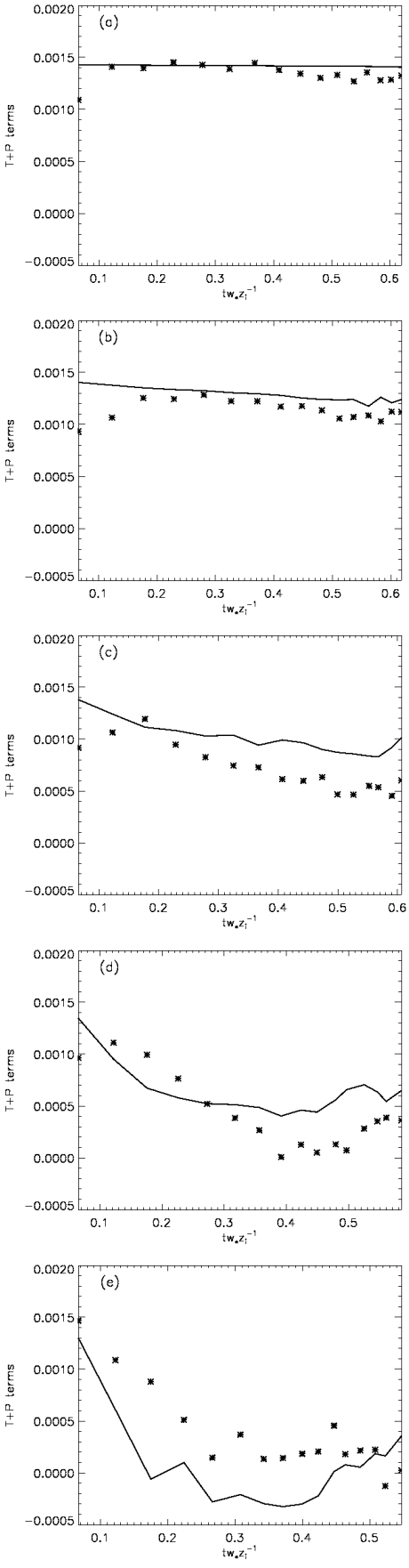

FIGURE 4: Transport and pressure ($T + P$) contributions to the TKE budget at z_i obtained by LES (asterisks) and by means of Eq. (5) (solid line) as a function of $tw_*z_i^{-1}$ for (a) NS, (b) GC5, (c) GC10, (d) GC15, and (e) GC20 cases.

Figure 4 shows the time evolution of transport and pressure contributions of the TKE at z_i for all the simulated cases obtained by means of LES (asterisks) and by using Eq. (5) (solid line). For all cases, the $T + P$ contribution decreases with increasing shear. When shear is large enough (GC15 or GC20) $T + P$ can be a sink of TKE at the inversion. For this reason, $T + P$ can not only scale with w_* and z_i (Eq. 6). When shear increases non–convective contribution which scales with local variables in the inversion zone (Eq. 7) reduces $T + P$ term. The proposed scaling (Eq. 5) approximately follows LES values for all of the simulated cases.

3.4.3 DISSIPATION CONTRIBUTION

Several different parameterizations have been proposed for this term. Some authors used a parameterization depending to stability of the air aloft, i. e., dissipation losses are proportional to the Brunt–Väisälä frequency. Others postulated that dissipation is proportional to buoyancy jump at the inversion (see Tennekes and Driedonks 1981 for a review). In recent years, dissipation was parameterized by assuming that its contribution is proportional to the production of TKE. As a consequence, this term was represented as a linear combination of the other TKE contributions (Flamant et al. 1999; Kim et al. 2006).

Two different dissipation processes can be identified at the entrainment zone (Zeman and Tennekes 1977; Tennekes and Driedonks 1981):

$$\epsilon = \epsilon_{NL} + \epsilon_L \tag{8}$$

First, it exists the dissipation process, following the turbulent energy cascade, of the large eddies that reach the inversion level. This contribution is related to the TKE values within the boundary layer. Similar to the scaling of the non-local contribution to the $T+P$ term (see previous subsection), this part reads:

$$\epsilon_{NL} = -C_{\epsilon 1}\frac{w_*^3}{z_i}, \tag{9}$$

with $C_{\epsilon 1} = 0.16$. Second, there is the dissipation of the small eddies locally produced by shear at the inversion. This local process has to scale with δ and $u_*|_i$ or ΔV_e. The proposed parameterization for this contribution is similar to the scaling of shear term, and reads:

$$\epsilon_L = -C_{\epsilon 2}u_*|_i^2\frac{\Delta V_e}{\delta}, \tag{10}$$

with $C_{\epsilon 2} = 0.5$. It is important to notice here that both contributions (convective and local) follow the classical scaling law of the dissipation (Tennekes and Lumley 1972).

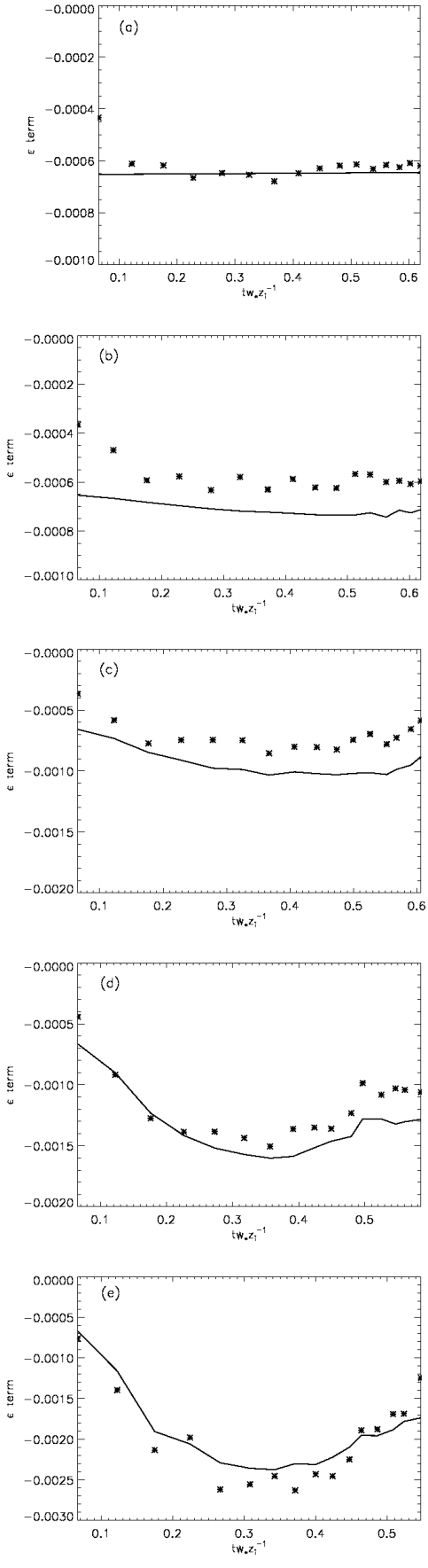

FIGURE 5: Dissipation (D) contribution to the TKE budget at z_i obtained by LES (asterisks) and by means of Eq. (8) (solid line) as a function of $tw_*z_i^{-1}$ for (a) NS, (b) GC5, (c) GC10, (d) GC15, and (e) GC20 cases.

Figure 5 shows the time evolution of dissipation contribution to the TKE at z_i for all the simulated cases obtained by means of LES (asterisks) and by using Eq. (8) (solid line). From the figure, one can conclude that ϵ contribution increases with shear and $|\epsilon_L| \gg |\epsilon_{NL}|$. When shear is large enough, the sum of transport and pressure terms of the TKE budget is an order of magnitude less than the other terms (see also figure 1) and approximately $-B = S + \epsilon$.

Regarding the proposed parameterizations obtained by using scaling arguments it is important to notice:

- The surface friction velocity u_* is not included in the parameterization of the shear or transport terms at the inversion. This marks a clear difference when compared to previous studies (see Conzemius and Fedorovich 2006b for a review). In our opinion, u_* at the surface does not have an explicit effect on the evolution of the TKE terms at the entrainment, at least for these cases where the entrainment zone begins to develop far from the surface layer. This can be shown by representing z_i against w_*. In this type of plot all the simulated cases regardless of the wind characteristics collapse in a single curve (not shown here). A similar result was pointed out by Conzemius and Fedorovich (2006a). If morning situations were considered, entrainment and surface layers are closer and u_* could have an influence on the entrainment processes.

- For shear–free CBL (NS case), the scaling parameters for all the TKE terms are z_i and w_*. For this case, $T + P$ and ϵ present the same kind of parameterization and the constant is $C_F - C_{\epsilon 1} = 0.19$, which is slightly lower than the typical value 0.2 for shear–free CBL. However, one can conclude that for this particular case $\beta(NS) < 0.2$ for most of the simulated period (not shown).

- Due to the similitude between Eqs. (4), and (10) when shear is included in the simulations, a unique constant, $C_M - C_{\epsilon 2} = 0.65$, can be used for the local entrainment contribution of $S + \epsilon$. That is, local and non–local dissipation contributions can be included in S and $T + P$ parametrizations respectively. For this reason, several authors did not explicitly consider the dissipation contribution in the virtual potential temperature flux ratio parameterization (Pino et al. 2003).

- For the shear generated turbulence in the entrainment zone, δ has been used as a length scale. Most of the authors used z_i and ΔV_e as scaling parameters. However, in our opinion, if ΔV_e or the local momentum flux, represented by $u_*|_i$, are used as velocity scales, the natural choice for the length scale is δ and not z_i (Stull 1976b).

- The boundary layer growth $\partial z_i / \partial t$ is not used as a scaling factor in any of the terms. If this variable is introduced in the scaling, in order to derive a parameterization for the virtual potential temperature flux ratio, an additional assumption, usually in a zeroth–order framework, has to be made to calculate this term (Lilly 1968; Tennekes 1973; Pino et al. 2003; Conzemius and Fedorovich 2006b; Kim et al. 2006).

4. CONCLUSIONS

The influence of shear on the evolution of a CBL was studied by means of large–eddy simulations. Since our main purpose was to deepen our understanding of the role of shear in the TKE budget at the entrainment zone, we performed five LES runs with varying wind shear conditions and analyzed the evolution of the different terms of the TKE budget. As previous studies found, our results have shown that the presence of geostrophic winds in convective situations enhances the entrainment flux by modifying the convection pattern specially at the entrainment zone. The larger entrainment fluxes generated with increasing wind shear produce a boundary layer that is warmer and drier. Therefore, the mixed–layer depth grows faster with increasing wind shear.

By means of the LES, it is possible to evaluate the various contributions to the TKE budget, and the influence of shear at the inversion is shown in the vertical distribution of the various terms of the TKE budget. The TKE budget for winds above 10 m s^{-1} shows that the shear term is the largest budget contribution in the entrainment zone. The other budget terms change when wind shear increases. The sum of transport and pressure terms decreases its value at the inversion level when shear increases. For all the prescribed sheared convective boundary layers, surface shear is no longer transported to the entrainment zone. That is, all the shear available for the entrainment is locally produced at the entrainment zone. The dissipation contribution presents a similar profile with height to shear. However, in the entrainment zone the dissipation alone is not able to compensate shear production; in large shear cases this shear excess is the main source of TKE.

These results were used to develop a representation, based on scaling, of the main contributions to the TKE budget. The broad variety of sheared CBLs observed in the atmosphere advise to enlarge the present study to different lapse rates or surface buoyancy heat fluxes. However, in view of the first results shown here, once each term is correctly fitted to the LES results, a preliminary parameterization of the virtual potential temperature flux can be built up and compared against LES results. Once the parameterization is checked for different CBL conditions, it can be implemented in boundary layer schemes to account explicitly for the shear contribution to entrainment.

The parameterization of each term fulfills the following properties. First, in the pure buoyancy case, the w_* and z_i are used as a velocity and length scales, respectively. Therefore, entrainment processes are affected by the bulk boundary layer and a convective scale produces

good results. In this case, a value of the entrainment virtual potential temperature flux ratio similar to the standard value $\beta = 0.2$ is obtained. Second, when shear is considered, non–convective (local) processes affect the entrainment properties of the TKE terms. In this case, apart from the convective scaling, local length and velocity scales have to be introduced. The natural entrainment length scale is the inversion layer thickness δ. For the entrainment scaling velocity several option arise. Once the boundary layer growth was not taken into account, the modulus of the inversion velocity jump ΔV_e, or a velocity inferred from the velocity flux at the inversion was considered. Third, a clear distinction of the processes which scale with integral CBL scales and those scaling locally have been made for all the analyzed TKE terms.

With respect to the scaling analysis, this parameterization is an improvement of the one presented by Pino et al. (2003) and incorporates the physical arguments of each TKE term not discussed by Kim et al. (2006) or Pino et al. (2006). The final parameterization fairly describes the simulated CBL evolution during the 8 hours of simulation.

Acknowledgments

This work was supported by the Stichting Nationale Computerfaciliteiten (National Computing Facilities Foundation, NCF) with the project SG–132 for the use of supercomputing facilities, with financial support from the Netherlandse Organisatie voor Wetenschappelijk Onderzoek (Netherlands Organization for Scientific Research, NWO) and Spanish MEC scientific projects CGL2005–07105 and ESP2005–062823–C05–03.

REFERENCES

Angevine, W. M., A. W. Grimsdell, A. McKeen and J. M. Warnock, 1998: Entrainment results from the Flatland boundary layer experiments. *J. Geophys. Res.*, **103,** 13689–13701.

Artaz, M. A. and J. C. André, 1980: Similarity studies of entrainment in convective mixed layers. *Bound.–Layer Meteor.*, **19,** 51–66.

Betts, A. K. and J. H. Ball, 1994: Budget analysis of FIFE 1987 sonde data. *J. Geophys. Res.*, **99,** 3655–3666.

Christian, T. W. and R. M. Wakimoto, 1989: The relationship between radar reflectivities and clouds associated with horizontal roll convection on 8 August 1982. *Mon. Wea. Rev.*, **117,** 1530–1544.

Conzemius, R. and E. Fedorovich, 2006a: Dynamics of sheared convective boundary layer entrainment. Part I: Methodological background and large–eddy simulations. *J. Atmos. Sci.*, **63,** 1151–1178.

Conzemius, R. and E. Fedorovich, 2006b: Dynamics of sheared convective boundary layer entrainment. Part II: Evaluation of bulk model predictions of entrainment flux. *J. Atmos. Sci.*, **63,** 1179–1199.

Cuijpers, J. W. M. and P. G. Duynkerke, 1993: Large eddy simulation of trade wind cumulus clouds. *J. Atmos. Sci.*, **50,** 3894–3908.

Cuijpers, J. W. M. and A. A. M. Holtslag, 1998: Impact of skewness and nonlocal effect on scalar and buoyancy fluxes in convective boundary layers. *J. Atmos. Sci.*, **55,** 151–162.

Culf, A. D., 1992: An application of simple models to Sahelian convective boundary–layer growth. *Bound.–Layer Meteor.*, **58,** 1–18.

Deardorff J. W. and G. E. Willis, 1982: Dependence of mixed–layer entrainment on shear stress and velocity jump. *J. Fluid. Mech.*, **115,** 123–140.

Driedonks, A. G. M., 1982: Models and observations of the growth of the atmospheric boundary layer. *Bound.–Layer Meteor.*, **23,** 283–306.

Driedonks, A. G. M. and H. Tennekes, 1984: Entrainment effects in the well–mixed atmospheric boundary layer. *Bound.–Layer Meteor.*, **30,** 75–105.

Dubosclard, G., 1980: A comparison between observed and predicted values for the entrainment coefficient in the planetary boundary layer. *Bound.–Layer Meteor.*, **18,** 473–483.

Fedorovich, E., 1995: Modeling the atmospheric convective boundary layer within a zero–order jump approach: An extended theoretical framework. *J. Appl. Meteor.*, **34,** 1916–1928.

Fedorovich, E., F. T. M. Nieuwstadt and R. Kaiser, 2001: Numerical and laboratory study of a horizontally evolving convective boundary layer. Part II: Effects of elevated wind shear and surface roughness. *J. Atmos. Sci.*, **58,** 546–560.

Fedorovich, E., R. Conzemius, I. Esau, F. K. Chow, D. Lewellen, C. –H. Moeng, P. Sullivan, D. Pino and J. Vilà–Guerau de Arellano, 2004: Numerical models of entrainment into sheared convective boundary layers evaluated through large eddy simulations. *16th Symp. on Boundary Layer and Turbulence,* Portland, MA, Amer. Meteor. Soc., 5.6.

Flamant, P., J. Pelon, B. Brashers and R. A. Brown, 1999: Evidence of a mixed–layer dynamics contribution to the entrainment process. *Bound.–Layer Meteor.*, **93,** 47–73.

Hägeli, P., D. G. Steyn and K. B. Strawbridge, 2000: Spatial and temporal variability of mixed–layer depth and entrainment zone thickness. *Bound.–Layer Meteor.*, **97,** 47–71.

Hunt, J. C. R. and P. A. Durbin, 1999: Perturbed vortical layers and shear sheltering. *Fluid Dyn. Res.*, **24,** 375–404.

Khanna, S. and J. G. Brasseur, 1998: Three dimensional buoyancy– and shear–induced local structure of the atmospheric boundary layer. *J. Atmos. Sci.*, **55,** 710–743.

Kim, S. –W., S. –U. Park and C. –H. Moeng, 2003: Entrainment processes in the convective boundary layer with varying wind shear. *Bound.–Layer Meteor.*, **108,** 221–245.

Kim, S. –W., S. –U. Park, D. Pino and J. Vilà–Guerau de Arellano, 2006: Entrainment parameterization in a

sheared convective boundary layer by using a first–order jump model. *Bound.–Layer Meteor.*, **120,** 455–475.

LeMone, M. A., 1973: The structure and dynamics of horizontal roll vortices in the planetary boundary layer. *J. Atmos. Sci.*, **30,** 1077–1091.

Lenschow, D. H., 1970: Airplane measurements of planetary boundary layer structure. *J. Appl. Meteor.*, **9,** 874–884.

Lenschow, D. H., 1974: model of the height variation of the turbulence kinetic energy budget in the unstable planetary boundary layer. *J. Atmos. Sci.*, **31,** 465–474.

Lilly, D. K., 1968: Models of cloud–topped mixed layer under a strong inversion. *Quart. J. Roy. Meteor. Soc.*, **94,** 292–309.

Mahrt, L. and D. H. Lenschow, 1976: Growth dynamics of the convective mixed layer. *J. Atmos. Sci.*, **33,** 41–51.

Moeng, C. –H. and P. P. Sullivan, 1994: A comparison of shear– and buoyancy–driven planetary boundary layer flows. *J. Atmos. Sci.*, **51,** 999–1022.

Pino, D., J. Vilà–Guerau de Arellano and P. G. Duynkerke, 2003: The contribution of shear to the evolution of a convective boundary layer. *J. Atmos. Sci.*, **60,** 1913–1926.

Pino, D., J. Vilà–Guerau de Arellano and S. –W. Kim, 2006: Representing sheared convective boundary layer by zeroth– and first–order–jump mixed layer models: Large–eddy simulation verification. *J. Appl. Meteor. Clim.*, **45,** 1224–1243.

Pino, D., and J. Vilà–Guerau de Arellano, 2008: Effects of shear in the convective boundary layer: Analysis of turbulent kinetic energy budget. *Acta Geophys.*, **56,** 167–193.

Sorbjan, Z., 1996: Effects caused by varying the strength of the capping inversion based on a large eddy simulation model of the shear–free convective boundary layer. *J. Atmos. Sci.*, **53,** 2015–2024.

Sorbjan, Z., 2004: Large–eddy simulations of the baroclinic mixed layer. *Bound.–Layer Meteor.*, **112,** 57–80.

Sorbjan, Z., 2005: Statistics of scalar fields in the atmospheric boundary layer based on Large–eddy simulations. Part 1: Free convection. *Bound.–Layer Meteor.*, **116,** 467–486.

Sorbjan, Z., 2006: Statistics of scalar fields in the atmospheric boundary layer based on Large–eddy simulations. Part II: Forced convection. *Bound.–Layer Meteor.*, **119,** 57–79.

Stull, R. B., 1976a: The energetics of entrainment across a density interface. *J. Atmos. Sci.*, **33,** 1260–1267.

Stull, R. B., 1976b: Mixed–layer depth model based on turbulent energetics. *J. Atmos. Sci.*, **33,** 1268–1278.

Stull, R. B., 1988: *An Introduction to Boundary Layer Meteorology*. Kluwer Academic Press, 670 pp.

Sykes, R. I. and D. S. Henn, 1989: Large–eddy simulation of turbulent sheared convection. *J. Atmos. Sci.*, **46,** 1106–1118.

Tennekes, H. and J. L. Lumley, 1972: *A First Course in Turbulence*. MIT Press, 313 pp.

Tennekes, H., 1973: A model for the dynamics of the inversion above a convective boundary layer. *J. Atmos. Sci.*, **30,** 558–567.

Tennekes, H., 1975: Reply to Zilitinkevich. *J. Atmos. Sci.*, **32,** 992–995.

Tennekes, H. and A. G. M. Driedonks, 1981: Basic entrainment equations for the atmospheric boundary layer. *Bound.–Layer Meteor.*, **20,** 515–531.

Zeman, O. and H. Tennekes, 1977: Parameterization of the turbulent energy budget at the top of the daytime atmospheric boundary layer. *J. Atmos. Sci.*, **34,** 111–123.

Zilitinkevich, S. S., 1975: Comments on “A model for the dynamics of the inversion above a convective boundary layer”. *J. Atmos. Sci.*, **32,** 991–992.

Zilitinkevich, S. S., 1991: *Turbulent Penetrative Convection*. Avebury Technical, 180 pp.